

Modeling capsid self-assembly: Design and analysis

D. C. Rapaport

Department of Physics, Bar-Ilan University, Ramat-Gan 52900, Israel

E-mail: rapaport@mail.biu.ac.il

Abstract.

A series of simulations aimed at elucidating the self-assembly dynamics of spherical virus capsids is described. This little-understood phenomenon is a fascinating example of the complex processes that occur in the simplest of organisms. The fact that different viruses adopt similar structural forms is an indication of a common underlying design, motivating the use of simplified, low-resolution models in exploring the assembly process. Several versions of a molecular dynamics approach are described. Polyhedral shells of different sizes are involved, the assembly pathways are either irreversible or reversible, and an explicit solvent is optionally included. Model design, simulation methodology and analysis techniques are discussed. The analysis focuses on the growth pathways and the nature of the intermediate states, properties that are hard to access experimentally. Among the key observations are that efficient growth proceeds by means of a cascade of highly reversible stages, and that while there are a large variety of possible partial assemblies, only a relatively small number of strongly bonded configurations are actually encountered.

Keywords: self-assembly, viral capsids, molecular dynamics simulation

PACS numbers: 81.16.Fg, 87.16.Ka, 02.70.Ns

1. Introduction

The formation of the capsid shells that package the genetic material of spherical viruses [1, 2] is a particularly familiar instance of self-assembly in the natural world, a phenomenon at the border between biology and physics. The rational design of antiviral agents would benefit from an improved understanding of how such shells assemble, while in the industrial environment molecular scale self-assembly is also expected to play a significant role in advancing nanotechnology. More generally, for a broad range of applications, structure formation in self-assembling molecular complexes is a particularly important process [3].

Experimentally, direct observation of evolving molecular assemblies is inherently difficult, with the final states revealing little about how they came into being. Strictly speaking, self-assembly also implies a nonequilibrium state, thus predictive theory (in the form of statistical mechanics) is absent. While simple mechanical models have been used to explore steric aspects of capsid assembly [4], an approach based on the

molecular dynamics (MD) simulation [5] of suitably designed models provides access to the assembly pathways themselves and a means for examining the possible existence of universal organizational principles that govern self-assembly. MD simulation is also able to predict the time-dependent populations of partial assemblies providing, in principle, a direct link with experiment [6].

The highly symmetric capsid shapes are a consequence of their being assembled from multiple copies of one or a small number of distinct capsomers [7]. Capsid assembly, a process whose details are little understood [8], is governed by different classes of interactions: There are interactions between the capsomers and the genetic material that initiate and regulate assembly, and subsequently stabilize the end product. More relevant for the present study are the protein-protein interactions between capsomers that are also important in stabilizing the shell structure. What makes capsid self-assembly suitable for simulation, despite the apparent biochemical complexity, is the fact that it is able to occur reversibly *in vitro* [9, 10, 11], without the genetic material that is essential to the virus *in vivo* (in other cases nucleic acid must be present [12]). In addition, structurally intact empty shells occur *in vitro* after removal of their contents, and viruses themselves form empty capsids [2]. Modeling is simplified considerably by such information, since only a very small number of well-characterized components need be considered.

Motivation for a reduced description stems from the robustness of self-assembly [4] and the prominence of icosahedral symmetry. Nature has adopted this structural motif precisely because the high degree of symmetry leads to a minimal set of construction specifications [1]; in addition, the almost spherical form offers near-maximal volume for a given surface area. Since the task of the genetic information embodied in the viral nucleic acid is not only to instruct the virus how to infect the host, but also to specify how it must replicate itself, if less information can be devoted to the latter mission, more will be available for the pernicious primary task. Analogous icosahedral motifs are to be found in geodesic domes, whose detailed structures are a consequence of the same minimalist construction specifications, as well as considerations of optimal rigidity. Beyond their basic packaging role, capsomers also have an important function in the virus life cycle [13] that lies beyond the scope of simple structural models.

MD modeling of capsid self-assembly, based on simple structural models that retain sufficient detail to ensure meaningful behavior, was introduced in Refs. [14, 15]. The principal characteristics of the approach are an effective molecular shape formed out of rigidly arranged soft spheres that enables particles to fit together in a closed shell, and multiple interaction sites positioned to stabilize the correct final structure. This highly simplified representation can be contrasted with real capsomers [7] that consist of intricately folded proteins whose exposed surfaces form relatively complex landscapes. The initial focus of the simplified approach was on achieving assembly; pathways were not investigated in detail, and solvent was omitted on account of computational limitations. Shells of size 60, formed from triangular and trapezoidal particles, were considered, the latter corresponding to T=1 viruses; even larger shells

of size 180, corresponding to $T=3$ viruses, were also grown. While the later stages of the work involved reversible assembly, a more reasonable approach from a physical perspective, the early part was based on irreversible assembly, again in order to reduce the computational effort.

The next step, extending the simulations to include an explicit atomistic solvent, had to await further increases in computing power [16, 17], but even so the simulations were limited to icosahedral shells constructed from triangular particles, rather than the larger shells considered previously. Solvent presence aids cluster breakup without subassemblies needing to collide directly, curtails the ballistic nature of the particle motion, and serves as a heat bath to absorb energy released by exothermal bond formation. The simulations revealed that self-assembly proceeded by means of a cascade of reversible stages, with a strong preference for low-energy intermediate states, eventually leading to a high proportion of fully assembled shells. While it may seem paradoxical, reversibility is the key to efficient production due to its ability to help subassemblies avoid becoming trapped in states off the correct pathway. These models, and some of their consequences, are explored below.

Other studies have also addressed capsid assembly dynamics. An alternative particle-based MD simulation involved quasi-rigid bodies formed from hard spheres [18]. Even simpler capsomer representations have been based on spherical particles, rather than the extended particle shapes considered here, with either directional interactions [19] whose range exceeds the particle size, or bonding energies determined by local neighborhood rules [20]; in these simulations the solvent is represented implicitly using stochastic forces. The motivation for using relatively complex particle designs, rather than simple spherical particles, is the fact that capsomers themselves are extended bodies whose customized shapes generally appear tailored to achieve properly assembled shells. The practical benefit of using model particles whose size is comparable to the interaction range is that the design ensures maximal bonding forces across interfaces between correctly positioned and oriented particles, while essentially eliminating bond formation in other situations. A similar outcome using spherical particles with directional interactions is less readily achieved, since the scope for tuning such designs to favor certain structural motifs – involving specific positions and orientations subject to narrow tolerance ranges – is more limited. Consequently, as demonstrated later, the present results show a strong preference for correct assembly, and even on the rare occasion that incorrect growth is initiated the unfavorable energetics ensures the transience of such structural defects.

Monte Carlo simulations of patchy spheres [21], tapered cylinders [22], and particles with force centers located at the vertices of polygonal pyramids [23] represent further alternatives, but here the dynamical aspects of assembly are absent. At the other extreme on the complexity scale are the all-atom descriptions of capsomer proteins, although such MD simulations [24] extend over very short time intervals, sufficient for testing the stability of preassembled shells. If the particle dynamics underlying self-assembly is not a consideration, then a range of theoretical approaches for studying

capsid structure exist [25, 26, 27, 28, 29], and experimental results have been interpreted using concentration kinetics [10, 30].

The present paper reviews some of the key aspects of the earlier MD work and provides early results from an ongoing effort to extend the approach. The organization is as follows: General considerations involved in modeling capsid construction are introduced, with details of specific designs, based on rigid soft-sphere assemblies, that give the particles their overall shape. The interactions responsible for structure formation are described, including alternative approaches based on both irreversible and reversible bonding. Assembly scenarios are then covered, together with the interaction restrictions that were necessary in the early stages of the work to supplement the interactions in the case of irreversible bonding. Computational techniques are summarized, followed by a selection of quantitative and visual results from past and current simulations.

2. Simulation methodology

2.1. Capsomer particle design

There are few guidelines to aid in the design of model capsomer particles apart from the need for the reduced representations to retain sufficient detail to ensure meaningful behavior when used in MD simulation. The two principal characteristics for the present work are the effective molecular shape, which must be tailored to ensure particles can fit together to form closed polyhedral shells, and the interactions between particles that drive self-assembly and maintain the structural integrity of partial assemblies and complete shells. The models introduced here are all based on rigid assemblies of soft-sphere atoms that give the particles their shape, together with precisely positioned attraction sites that ensure particle pairs are properly positioned and aligned when in their minimal energy bound states. General thermodynamic considerations aid in choosing the force parameters, but otherwise the approach is entirely empirical and the parametrization is not tied to any particular experimental measurements. Progress in discrete particle modeling of this kind is determined by available computer power, with increasing computational capability allowing the incorporation of additional features to enrich the model, as well as permitting the larger systems and longer runs that may be needed to establish behavior.

The initial study [14] considered rigid triangular particles, shown in Fig. 1, designed for assembly of 60-faced pentakis-dodecahedral shells. The overall shape is produced by the arrangement of the larger spheres. The repulsive force between spheres in different particles, used to prevent spatial overlap, is based on the truncated Lennard-Jones potential

$$u(r) = \begin{cases} 4\epsilon[(\sigma/r)^{12} - (\sigma/r)^6 + 1/4] & r < r_c = 2^{1/6}\sigma \\ 0 & r \geq r_c \end{cases} \quad (1)$$

where r is the sphere separation, σ approximates the sphere diameter, ϵ determines

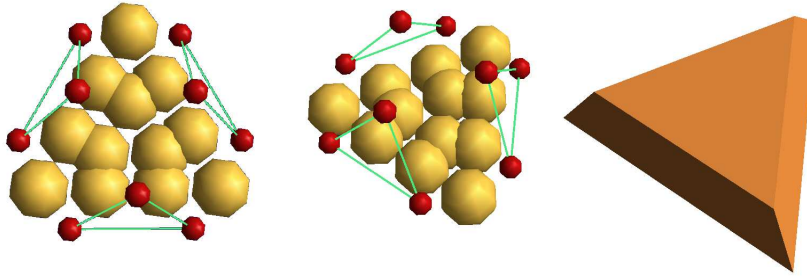


Figure 1. (Color online) Details of the original model capsomer particle, with the large spheres that provide the excluded volume and the small spheres denoting attraction sites; the equivalent triangular block is also shown, with beveled lateral faces that allow formation of a 60-faced polyhedron from multiple copies of the particle, using irreversible bonding.

the energy scale, and r_c is the interaction cutoff. In the reduced MD units used here, $\sigma = \epsilon = 1$; thus the spheres that give the particles their shape are of approximately unit diameter. While there are multiple interactions between the spheres belonging to particles that are in close proximity, the computations based on pair potentials are simpler than evaluating the overlap of complex rigid bodies required by alternative shape representations.

The small spheres in Fig. 1 signify attraction sites, three per face, and extending beyond the volume occupied by the spheres that give the particle its shape (towards the shell interior when particles are correctly positioned); corresponding pairs of attraction sites on different particles interact through an inverse-power potential and at close range this interaction smoothly merges into a narrow harmonic well (see details below). Successful assembly involves the coupling of each of the complementary pairs of attraction sites, and is conditional upon particles having the appropriate dimensions to ensure components fit together, with the angles of the planes containing the attraction sites determined by the overall shell shape.

Subsequent work [15] involved models that extended this basic design. Shells corresponding to a T=1 virus are constructed from 60 identical trapezoidal capsomer particles shown in Fig. 2. The shell can be regarded as an icosahedron [31] each of whose 20 equilateral triangular faces is subdivided into three coplanar trapezoidal units. The lateral particle faces within the triangle are normal to the triangular plane, whereas those along the outside of the triangle are inclined at 20.905° to the normal, resulting in a dihedral angle of 138.190° ; these angles dictate the positioning of the attraction sites. Each of the three short edges contains a single set of attraction sites, while the long edge contains two sets.

A further increase in complexity is the T=3 shell consisting of 180 trapezoidal particles. This shell is based on a rhombic triacontahedron [31] with 30 identical rhombic faces; each face is subdivided into two isosceles triangles (the base angles are 58.283° , so the triangles are almost equilateral), and each of these triangles is then divided into three

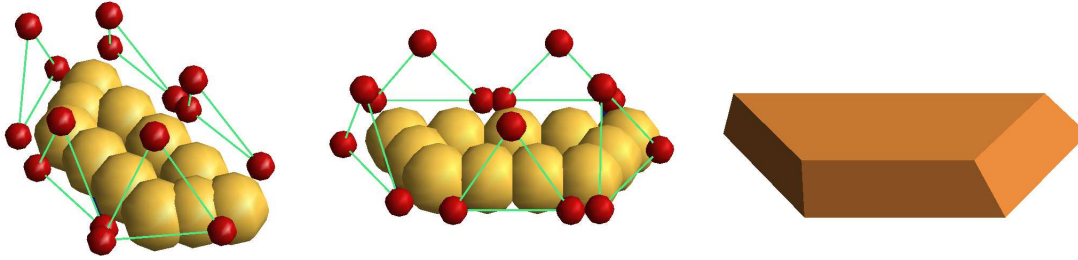


Figure 2. (Color online) Capsomer model used for $T=1$ assembly with irreversible bonding; the spheres comprising the particle and the effective trapezoidal shape are shown.

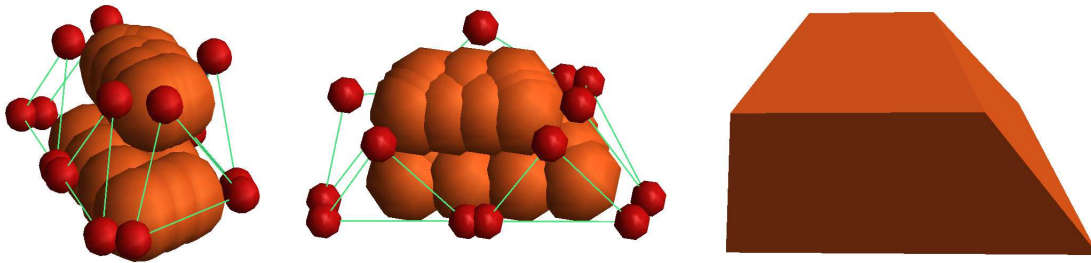


Figure 3. (Color online) Views of $T=3$ capsomer model.

coplanar trapezoidal particles. The lateral faces within the same triangle, and between the triangles comprising the rhombus, are normal to the triangular plane, while the other faces are inclined at 18° , producing a dihedral angle of 144° . The particle is shown in Fig. 3. Note that two layers of spheres are now used to increase the overall thickness of the particle in order to help avoid unwanted interactions.

Since 60 is the maximum size under conditions of complete equivalence, the construction of larger structures is explained by employing the concept of quasi-equivalence [2, 32, 33]. Quasi-equivalence requires an autosteric mechanism, in which capsomer protein conformation varies by a small amount [34] depending on the position in the shell (mechanical analogies are discussed in Ref.[4]). However, the model designs used here assume a fixed shape. To overcome this difficulty, three particle variants with slightly different face angles are used (with attractive interactions only between corresponding face pairs), each destined to occupy a different subset of locations (corresponding to the subdivision of the isosceles triangles into trapezoids) within the shell.

The labeling scheme used for the sets of attraction sites is shown in Fig. 4. For $T=1$ the trimer takes the form of an equilateral triangle, whereas for $T=3$ a small change of apex angle is needed that makes the triangle isosceles. Since color coding is useful for $T=3$, particles are labeled B, G, R (blue, green, red) following [12]. The five sets of attraction sites follow the same bonding pattern in each particle, namely,

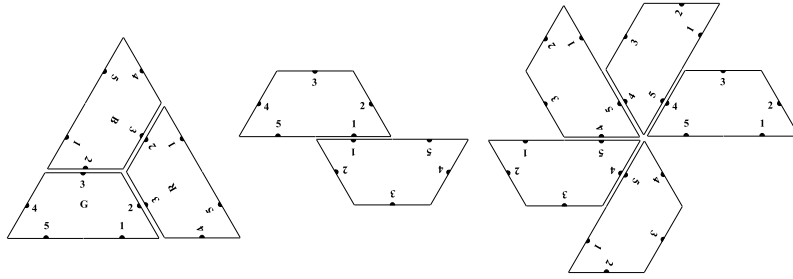


Figure 4. Trimer, dimer and (opened-up) pentamer configurations with labeled attraction sites; the color identification (used for $T=3$) is included in the triangular configuration.

complementary site pairs in sets 2 and 3 can bond, as is also the case for sets 4 and 5, while sites in sets 1 bond with each other. Different site pairings are associated with trimer, dimer, and pentamer or hexamer formation. Three particles joined by 2-3 bonds produce a planar triangular trimer. The 1-1 bonds form a dimer; it is nonplanar for $T=1$, while for $T=3$ it is planar when two type G particles are involved and nonplanar in the alternative R-B case. The 4-5 bonds produce a nonplanar, flower-like pentamer for $T=1$. On the other hand, for $T=3$, there are again two possibilities; if all particles are of type B they produce the pentamer, but a hexamer is formed when alternating R and G types are involved (appearing as three coplanar pairs).

The particles described so far were used in studies of irreversible assembly. Reversible bonding was also considered in Ref. [15]. Fig. 5 shows the design used for $T=1$ shells in this case. Constructing the particle from three layers of spheres reduces even further the likelihood of incorrect bonding; this is now a more important issue since there are no restrictions (see below) to help avoid attractive interactions that do not contribute to the final shell. Each bond now involves four attraction-site pairs; the energetic gain of a correctly aligned state is enhanced by distributing the interactions over more site pairs. Owing to the increased particle thickness, attraction sites can now be positioned so they no longer extend beyond the actual area of the lateral faces; the additional steric screening helps prevent unwanted interactions. Such benefits come at the price of increased computational effort.

Figs. 6 and 7 show the complete shells that these particles are designed to form (the images are of shells produced by the simulations). The former shows a $T=1$ shell; due to the nature of the bonding forces (see below) complementary attraction sites coincide in the ground state, although in the figure particle size is slightly reduced so the bonds can be seen. The latter shows a $T=3$ shell formed from the three different particle types; here particles are drawn to show their effective sizes, hiding the bonds. The different local particle arrangements described previously are all visible.

More recent simulations [16, 17] involving both reversible bonding and an explicit solvent have been confined to icosahedral shells, the reason once again being computational. Particles have an effective shape of a truncated triangular pyramid,

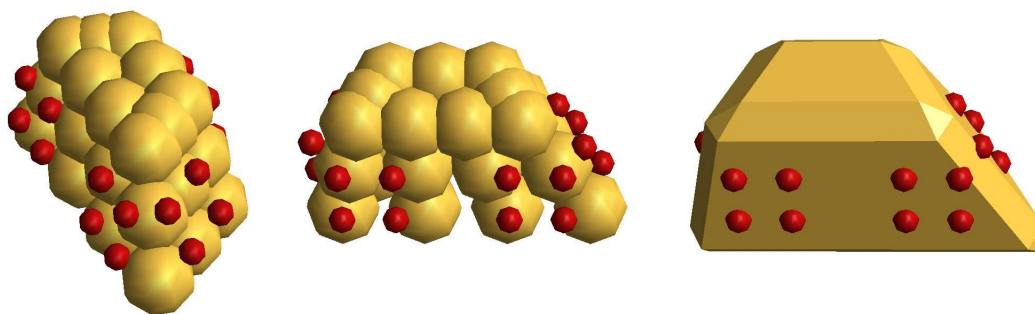


Figure 5. (Color online) Views of capsomer model used for $T=1$ reversible bonding.

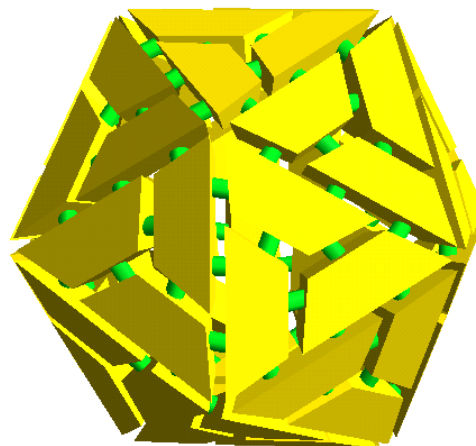


Figure 6. (Color online) Complete $T=1$ shell with 60 particles; particles are shown slightly reduced in size to allow the bonds to be seen.

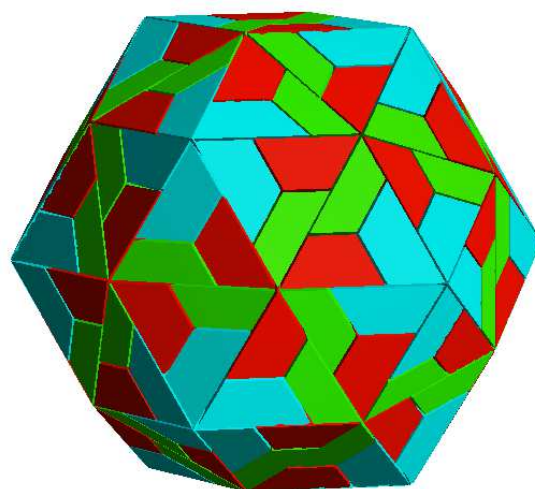


Figure 7. (Color online) Complete $T=3$ shell with 180 particles of three (color-coded) types.

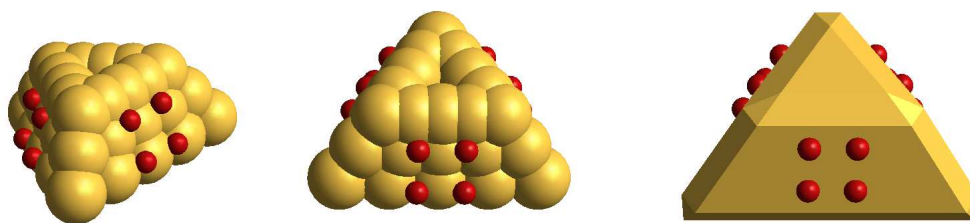


Figure 8. (Color online) Model particle and its effective truncated pyramidal shape used for assembly with an explicit solvent.

shown in Fig. 8, with multiple layers of spheres again used for steric shielding of the attractive interactions. The lateral faces containing the attraction sites are inclined at 20.905° . The volume of this particle should be contrasted with the one shown in Fig. 1 that consists of a single layer of spheres.

These represent the simplest of designs and there are, of course, numerous ways of enhancing the models. One example is the introduction of more complex particle surfaces, allowing the use of a ‘lock and key’ mechanism to represent additional steric effects. An attempt was made to use such a technique in early work on small triangular particles, by adding an extra sphere to the center of a lateral face and leaving a vacancy in the complementary face, but this mechanism failed to provide sufficient extra rigidity. The subsequent increased size and multiple attraction sites of the larger particles appear adequate for the present work.

2.2. Bonding interactions

Bond formation between real capsomers involves contributions from a relatively large number of pairs of interaction sites distributed over the mutual contact surface between the proteins. Although such interactions are not individually directional, in view of the substantial size of the capsomer compared to the effective interaction range, it is unlikely (and disadvantageous) that the interactions would be able to produce strongly bound states in which capsomers are incorrectly aligned. This is not necessarily true for simplified models with few attraction sites and an overall capsomer particle size similar to the interaction range; in this case, small clusters can become trapped in states corresponding to spurious local energy minima instead of developing into complete shells. Ensuring defect-free assembly can be accomplished by a trade off between model particle size and interaction complexity (with possible supplementary restrictions governing when and where attraction is allowed). The models used in the present series of studies demonstrate how increasing the particle size (at increased computational cost) relative to the interaction range allows the interaction details to be simplified (and other artifacts eliminated).

Two fully-bonded particles are held together by interactions between multiple (three or four) pairs of complementary attraction sites. Typically, particles might be

drawn together initially by just one of the attraction site pairs, and they then reorient so the remaining site pairs can participate. The use of multiple sites, where only complementary sites can interact, helps accomplish several goals: (a) The orientation of a lateral face and, consequently, the preferred dihedral angle between particles, is determined by the plane containing the sites. (b) The overall bonding interaction is distributed over the contact face; this ensures that the total bonding energy of misaligned particles can only be a fraction of the value in the ground state, thereby reducing the stability of improper bonds. (c) Multiple attraction sites enhance structural rigidity by suppressing internal degrees of freedom such as twisting or flapping.

The functional form of the interaction between bond-forming attraction sites, chosen entirely for convenience, is a negative power of the site separation r (e.g., $1/r^2$) when the sites are not too close, and for $r < r_h$ it takes the form of a narrow harmonic well; in the minimum energy state $r = 0$ and the attraction sites coincide. In the case of reversible bonding, the force is derived from the potential

$$u(r) = \begin{cases} e(1/r_a^2 + r^2/r_h^4 - 2/r_h^2) & r < r_h \\ e(1/r_a^2 - 1/r^2) & r_h \leq r < r_a \end{cases} \quad (2)$$

with typical parameter values $e = 0.1$ (in the case of reversible bonding the effect of varying the interaction strength parameter e is investigated – see below), $r_h = 0.3$, and cutoff $r_a = 3$ (in the solvent-free work $r_a = 2$). Particle size exceeds the interaction range, although less so than in real capsomers; the effect of a relatively short-ranged force, together with multiple attraction sites, is to reduce the attraction between wrongly positioned or oriented particles.

The interactions used with irreversible bonding are similar, the principal difference being that a permanent bond forms the first time $r < r_h$. Following the formation of this bond only the harmonic component of the attraction acts, irrespective of r , implying an infinitely high barrier to bond breakage. Earlier work also included an explicit torsional interaction to accelerate the bonding process, but this was eliminated once it became apparent that multiple pair interactions alone were adequate for achieving correct particle orientation.

Preferred assembly pathways are another feature meriting study. Since the likelihood of two arbitrary subassemblies being able to mesh successfully is low (unless incompatible pieces can be discarded in the process – possible only if bonds can break without too much effort), a hypothetical assembly scenario can be based on a multistage process, with small clusters of particles having a specified organization forming initially, and then combining into increasingly larger subassemblies. These small clusters must be able to ‘tile’ the complete shell, so a possible first stage is the assembly of triangles from the trapezoidal particles, while in the second stage these trimers bond to form full shells. Experimental signatures of multistage assembly would be certain preferred intermediate cluster sizes, or the more accessible rate concentration dependence [10, 35]. While it is not possible to enforce such behavior strictly by choice of interactions alone (it can be achieved using assembly restrictions – see below), increasing the interaction

strength e for those bonds responsible for (e.g.) trimer development can help bias the growth pathway in the correct direction.

2.3. Computational details

General MD methodology is discussed in Ref. [5]; a brief summary of the issues relevant to capsomer self-assembly simulation follows. Interaction calculations are carried out using neighbor lists, with the list construction following the procedure used for monatomic fluids. Separate lists are used for the short-range repulsive forces between the spheres that give the particles their shape, and for the longer-range forces between attraction sites. The rotational equations of motion employ standard rigid-body methods; these, together with the translational equations, are solved using a leapfrog integrator, with a time step of 5×10^{-3} (in reduced MD units).

The earlier simulations did not include a solvent (a simplification motivated by the fact that it is often adopted in modeling protein folding); even the simplest atomistic solvent would increase the computational effort substantially, not only because of the additional elements involved in the simulation, but also because of the slower particle movement when in a solvent rather than in a vacuum. To ensure an adequate supply of unbonded particles in the solvent-free simulations, partial shells below a certain size threshold were broken up at regular intervals (with a frequency depending on growth rate) by switching off their bonding interactions for a short period.

Later simulations included an explicitly modeled solvent. The solvent atoms are identical to the particle spheres, and are subject to the same soft-sphere repulsion. The mass of each particle is proportional to its volume, here typically $21 \times$ the solvent atom (whose mass is unity in MD units); having a much smaller mass ratio than in real viruses reduces the assembly timescale, making it more accessible to MD without any qualitative change in behavior expected. Particle concentration is much higher than in reality, but there is adequate solvent present to ensure that the ballistic particle motion of the solvent-free case is now dominated by diffusion.

Although the interactions between particles incorporate an attractive component, the only interactions involving solvent atoms (both among themselves and with the particles) are due to excluded volume; while this is a major simplification compared to actual capsomers in aqueous solution, it is reasonable to expect that the essential features of self-assembly are preserved. A more focused program of experiment and simulation will be needed for systematically determining which properties of the capsomers and their environment are necessary for the assembly process and which play a more passive role.

Two kinds of boundary conditions have been used. Because of the importance of visualization (including animation), early work used elastically reflecting hard walls, implemented using short-range repulsive forces that act perpendicularly to the surfaces; this avoids the sometimes confusing imagery that accompanies periodic boundaries. Later work, with larger systems, returned to conventional periodic boundaries, with the

minor visual artifacts associated with particles residing close to region boundaries no longer a significant issue.

In the initial state, particles and solvent atoms (where present) are positioned on a lattice; each is assigned a random velocity, and the particle orientation is also set randomly. The lattice spacing is determined by the overall number density of the system; if there is a risk of overlap at the start, particles can begin as collapsed objects (the size of a single sphere) and allowed to expand gradually to their final shape over the initial (e.g.) 5000 steps.

Exothermal bond formation will heat the system; this problem is particularly acute when there is no solvent due to the limited number of degrees of freedom capable of absorbing the excess thermal energy. Applying a weak damping force, $-\gamma (\vec{v} \cdot \vec{r}) \vec{r}/r^2$, along each bond resolves this issue, where \vec{v} is the relative velocity of the attraction sites and the damping coefficient $\gamma = 0.1$ (typically). Use of constant-temperature MD then ensures that the overall temperature does not change despite bond formation and damping; the net effect is to transfer energy associated with internal cluster vibration to the motion of entire clusters. The problem is less severe when a solvent is included, but the thermostat is still required, and is used to maintain a temperature of 0.667, corresponding to unit mean particle kinetic energy (translational and rotational); the damping force is no longer required in this case.

The interaction parameters are chosen to achieve efficient self-assembly while maintaining numerical stability; there is presently no relation to experimental association energies [34]. The number density ρ affects the outcome and must also be established empirically (here $\rho \leq 0.2$). Too high a value of ρ will not provide adequate space for shells to grow without mutual interference, whereas if ρ is too low, growth is retarded due to particles tending to lie beyond their attraction range and the lack of collisions that can, in the case of reversible bonding, help break off incorrectly bound pieces from partially formed shells.

2.4. Supplementary interaction restrictions

In the initial work, confined as it was to smaller particles, with severe computational limitations demanding rapid assembly and high yield (not necessarily a requirement *in vivo*), the need to resort to irreversible bonding for efficiency reasons required supplementary restrictions as to when bonding interactions were allowed to act. Their purpose is the avoidance of construction errors that could not be rectified subsequently; these errors, in turn, would lead to mutant structures and even amorphous clusters.

With the benefit of considerably more powerful computers (not to mention a little hindsight), these additional conditions are no longer needed for modeling assembly at the current level of description, with bonds now simply regarded as potential wells of finite depth. Nevertheless, it is worth considering these restrictions; the ideas they embody may prove useful at some future stage, and some of the mechanisms themselves may be physically justifiable as they could manifest themselves through local conformational

variation in response to changes in bonding state. The alternative approaches based on irreversible and reversible bonding represent, respectively, the extremes of kinetically limited and equilibrium assembly.

One simple restriction is that after a permanent bond has formed, the attraction sites involved no longer interact with other particles. Since several site pairs are involved in drawing a pair of particles into a bound state and a certain amount of time can elapse between the first and last pairings, the risk of forming incompatible bonds is reduced if neither of these particles can attract new particles until bonding of all the site pairs is complete. If construction follows a pathway in which, for example, dimers form initially, and then bond into larger structures, an analogous condition is applied to entire dimers.

To minimize any adverse effects, if bonding fails to complete within a prescribed interval (here, 4000 time steps) the existing partial bond is broken; immediate rebonding of the separated particles is prevented by requiring them to wait 1000 steps before becoming available for bonding again. The aim of additional mechanisms of this kind is to help ensure the release of particles that are unable to bond completely, as in the case when two particles attempt to bond along different exposed faces of a cluster opening big enough for just one of them. Yet another restriction, introduced for computational convenience, is that particles permanently bound into different partially formed structures do not attract one another, but only unbound particles; this avoids issues of structures not being able to mesh correctly. Finally, to ensure that enough particles are available for populating the complete shells, only a limited number of subassemblies are allowed to begin the growth process.

Other interaction restrictions can be used to enforce assembly pathways; thus if growth occurs via trimer intermediates, particles are first required to form trimers, and only clusters with all their internal bonds complete are allowed to associate into larger structures. Additionally, by restricting the number of larger subassemblies that can nucleate (e.g.) by the joining of two trimers, equivalent to a rate-limiting process [10], it is possible to enhance the yield of complete shells rather than numerous small fragments. Owing to the intrinsic bond flexibility, the need for further restrictions only becomes apparent as incorrect structures appear in the simulations; in some cases the restrictions are used to enforce particular bonding sequences to prevent partially bonded particles from encountering inappropriate bonding partners [15]. As indicated earlier, use of reversible bonding eliminates such issues.

3. Results

3.1. General aspects

System sizes and run lengths varied over a wide range. In the early work, with irreversible bonding and no solvent, the T=1 simulations used 1000 particles, with 13 shells allowed to develop and run lengths of up to 3×10^5 time steps, while for the larger T=3 shells there were 4096 particles, 10 shells allowed to develop and run lengths up

to 8×10^5 steps. The $T=1$ case, with reversible bonding and no solvent, also included 4096 particles, but the run length was extended to 10^7 steps; while there was no limit on the number of shells allowed to grow, partial assemblies of size ≤ 30 were broken up every 5×10^5 steps by turning off their attractive interactions over the subsequent 10^4 steps. At the other extreme, simulations involving reversible bonds and a solvent consisted of 1875 triangular particles – sufficient for 93 full shells – and solvent atoms bringing the total to 125 000; the required run lengths sometimes exceeded 70×10^6 steps. Thus, between the original and the latest work, the overall computational effort per run expanded over several orders of magnitude, with the longest runs requiring extended periods (measured in weeks) of computation using workstations with dual 3.6GHz Intel processors able to compute approximately 10^6 steps per day.

The selection of results shown here for the early solvent-free work is limited to images produced during the simulations that lead to the growth of $T=1$ and $T=3$ shells. The main focus of more recent simulations that include solvent is on the growth of smaller shells; the analysis carried out for these systems is more detailed, with emphasis on quantitative results. Current simulations, described briefly at the end of this section, attempt to address larger shells once again.

To allow post-analysis of the simulations, a sequence of ‘snapshots’ is recorded at intervals of 2000 steps over the duration of each run. Shell properties can be measured directly from this retained data, allowing the average growth statistics to be analyzed, together with the behavior of individual shells. Time resolution is limited by the snapshot interval, so that shortlived bonds between snapshots will be overlooked, as will merged events such as two added monomers that are indistinguishable from dimer addition. However, since particles move relatively slowly on the MD time scale, significant changes generally take sufficiently long for the majority of individual growth steps to be identified.

3.2. Shell analysis

Algorithmically establishing the identities of particles that are members of partial assemblies and verifying that shells are correctly assembled requires the capability for identifying bound clusters [5] and checking the connectivity of their bond networks. With reversible bonding, there is a certain amount of arbitrariness in defining what constitutes a bound particle pair. Individual attraction sites are regarded as bonded when they are separated by a distance < 0.6 ($= 2r_h$), an empirically chosen threshold that avoids transient bond breakage and reformation due to the thermal vibrations. Particles are considered bound if all four complementary site pairs are bonded, a state that also implies alignment owing to the relatively tight tolerances in the design. In view of the comparative rigidity of multiply-bonded subassemblies, a cluster corresponds to a closed shell if the numbers of particles and bonds equal the expected values, a criterion that can also be verified visually. Completely closed shells are subject to only the smallest of fluctuations in the relative particle positions and orientations.

Describing the nature of incomplete shells, while straightforward when the imagery is available – a nearly complete shell is readily characterized, as is a shell with a localized defect – is not obviously quantifiable. Since partially formed structures, and defect-free shell fragments in particular, have a variety of morphologies, automated classification is a nontrivial task. Each such structure can be represented as a bonded network, or graph, and while it is possible to determine the graph topology by examining connectivity, and the cluster compactness by counting missing bonds, it is not apparent how such information can be utilized. Furthermore, it turns out that growth is not necessarily a process in which shells grow monotonically by accretion of individual particles or small subassemblies; indeed, larger subassemblies can be seen to aggregate and (under reversible bonding conditions) groups forming partial shells do manage to break away from larger structures. Results obtained from the limited quantitative techniques available are described here, and these will be followed by visual examples of some of the more interesting, and complex, assembly events.

The most important observation regarding the overall behavior, applicable to both irreversible and reversible bonding alike, is that polyhedral shells have little difficulty growing to completion, and mutant structures are highly unlikely. Partial shells tend to have few voids in their surfaces, and shells nearing completion typically have a minimal number of openings; more open cagelike structures with multiple lacunae tend to be avoided. The results also reveal, not surprisingly, that an inappropriate choice of interactions, or even a slight error in defining particle geometry, leads to a wide variety of alternative structures, including open networks, incorrectly linked assemblies of shell fragments and other ill-characterized shapes.

A goal of this work is to identify particle designs that produce a high yield of properly assembled shells. The fact that incorrect assembly features more prominently in [19] is attributable to the fact that spherical particles with directional interactions are limited in their ability to exclude incorrectly bonded structures, while in [18] a similar outcome is due to the inherent flexibility of the linked structures that are used instead of rigid particles. Even further reduction of the structural preferences, as in the case of tapered cylinders [15], leads to a broad distribution of shell sizes, since packing considerations are only able to impose partial ordering on the particles, the exact opposite of the strong structuring of the present approach.

The stored snapshot data can be used to produce animated sequences that provide condensed summaries of the runs in full three-dimensional detail; this is very helpful for extracting more subtle, and not readily quantifiable features of the growth histories, examples of which are discussed below. Fig. 9 shows several images of $T=3$ growth with irreversible bonding and a dimer-weighted pathway, as extracted from the snapshot sequence (the color scheme differs from Fig. 7). Images from the much longer, reversible, solvent-free $T=1$ case are shown in Fig. 10.

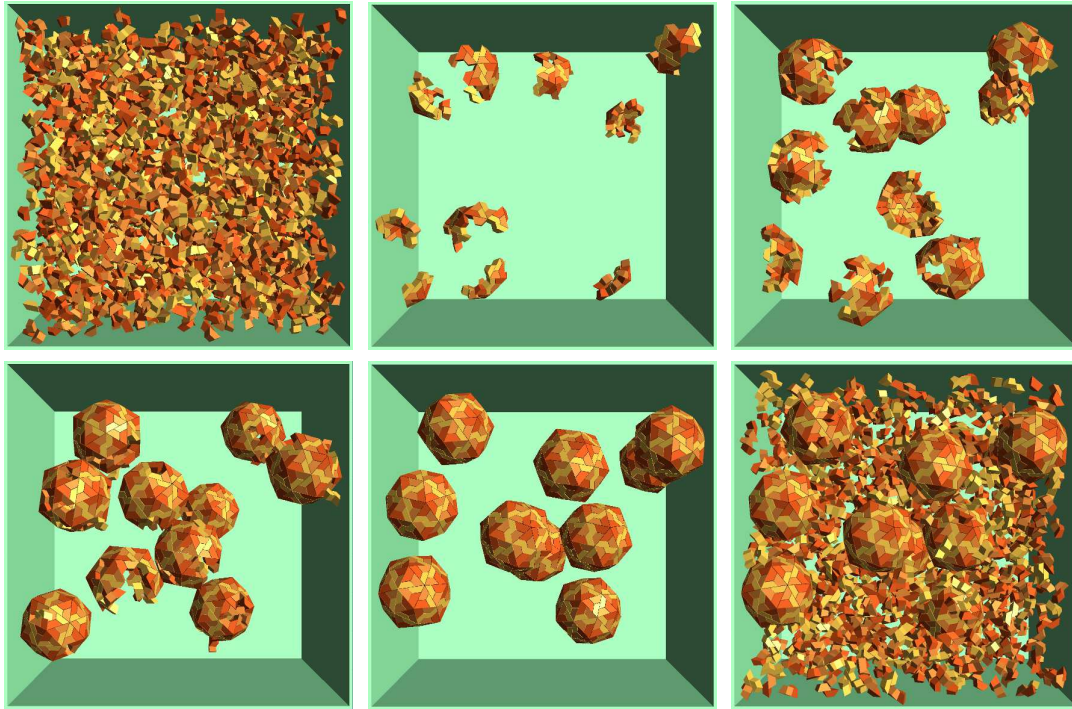


Figure 9. (Color online) Snapshots from a $T=3$ simulation with irreversible bonding: the frames show an early state, four views at different times including the final state showing only the shells, and the entire system in the final state (particles are color-coded by type).

3.3. Shell growth

The viability of the method is based on its ability to produce complete shells. Examples of the successful outcome of solvent-free simulations, both irreversible and reversible, have been described visually. The more detailed quantitative results that follow are for icosahedral shell growth under reversible bonding conditions and in the presence of a solvent. In this series of simulation runs the dependence on the interaction strength e is studied systematically. If the range of variation is not too large this is equivalent to examining the temperature dependence of the behavior. While the coverage of the phase diagram is limited (other parameters defining the model have been sampled more sparsely), it is more than adequate for demonstrating a selection of very different outcomes.

Table 1 provides a concise summary of these runs. The results are expressed as the mass fraction of particles contained in complete shells, in clusters of different size ranges, and the remaining monomers. Runs are sufficiently long for the cluster populations to stabilize.

At a low value, $e = 0.11$, there is practically no growth, due to minimal initiation. The yield increases with e , and production efficiency peaks at $e = 0.13$, with a yield of 83 shells, out of a maximum possible 93. At higher $e - 0.14$, and especially $0.15 -$ the

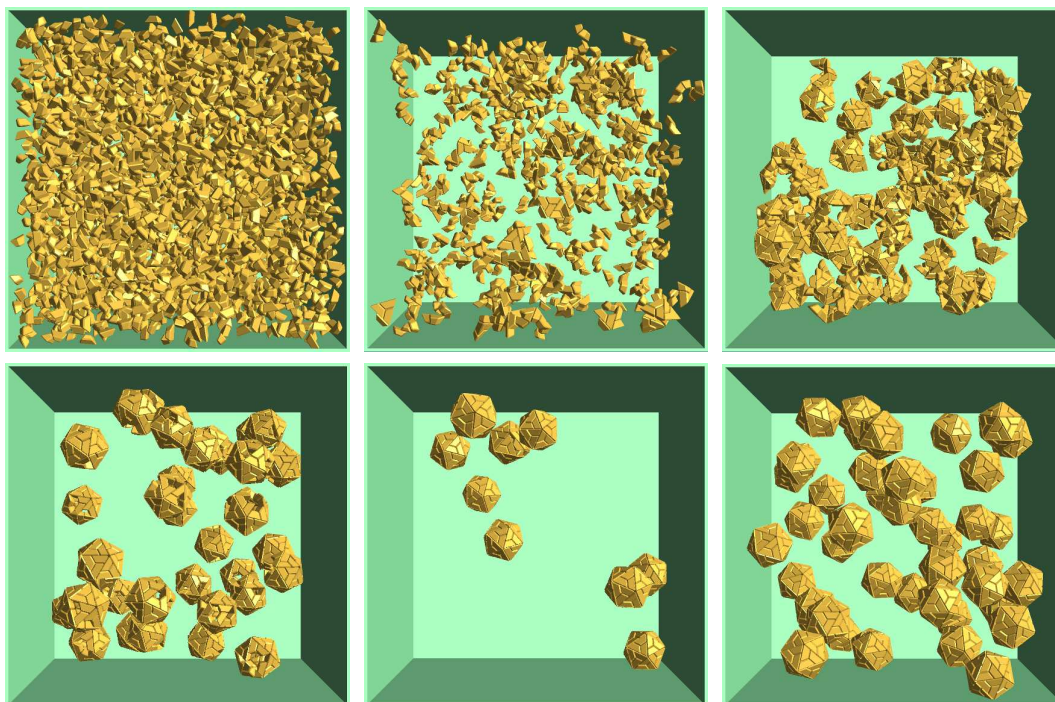


Figure 10. (Color online) Snapshots from a $T=1$ simulation with reversible bonding but without solvent: the frames show the entire system near the start of the run, 366 clusters of size ≥ 2 after 10^5 steps (monomers are not shown), 68 clusters of size ≥ 20 after 3×10^5 steps (smaller clusters are not shown), 33 clusters of size ≥ 50 after 10^6 steps, 9 complete clusters (size 60) after 3×10^6 steps, and final state with 46 complete clusters after 10^7 steps.

Table 1. Final cluster distributions for different interaction strengths e ; the results show the monomer mass fraction, the clusters grouped into two size ranges, and the complete shells, with the maximum mass fraction for each run in bold.

e	Cluster mass fraction			
	Size: 1	2-14	15-19	20
0.11	0.7931	0.1157	0.0165	0.0747
0.115	0.5153	0.1013	0.0101	0.3733
0.12	0.3040	0.0346	0.0000	0.6614
0.125	0.1915	0.0518	0.0101	0.7466
0.13	0.0709	0.0278	0.0160	0.8853
0.14	0.0011	0.0774	0.2922	0.6293
0.15	0.0000	0.1990	0.5983	0.2027

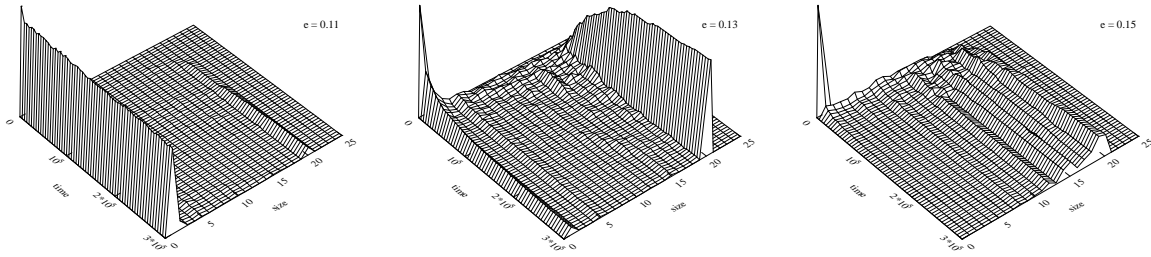


Figure 11. Cluster size distributions as functions of time (MD units); the distributions, including monomers, are expressed as mass fractions, and e (attraction strength) values are selected to show three distinct growth scenarios.

ability to reach completion is inhibited by excessive early growth, resulting in too many monomers being incorporated into clusters prematurely. No oversized (mutant) clusters are encountered here, although they would be expected for sufficiently large e . While similar overall behavior is seen in reaction kinetics studies [10], provided nucleation is rate limited, MD needs no restrictions of this kind.

Examples of the time-dependent cluster size distributions appear in Fig. 11. The values of e shown are selected to illustrate the different kinds of behavior. When closed shells are produced in significant number, the yield curves (i.e., the mass-fraction values for size 20) as a function of time have the familiar sigmoidal shape – rapid production after an initial delay that eventually tapers off. It is also abundantly clear from Table 1 and Fig. 11 (see also [16]) that in high yield runs there are very few clusters of intermediate size remaining at the end, essentially only complete shells and monomers. This is one of the key observations to emerge from these simulations.

Fig. 12 shows the outcome of a run with 2750 triangular particles, together with solvent, at a lower density ($\rho = 0.1$) and with $e = 0.14$; after 45×10^6 steps 105 out of a possible 137 closed shells have formed. Other partial structures (and monomers) are shown semi-transparently. Note that periodic boundaries are applied at the level of individual particles, so that shells crossing the region boundaries appear fragmented; solvent particles are not shown here (for clarity), but they fill the volume.

The stability of complete shells was tested by extending this particular run, once it had produced the large shell population, after reducing e to a value where assembly would normally yield only a few dimers at most. The residual small clusters promptly vanished, followed by the gradual disappearance of larger partial shells; eventually only the original fully closed shells remained, together with the occasional dimer. This is a demonstration of hysteresis [36], the enhanced stability and consequent survival of complete shells, even when growth conditions become unfavorable.

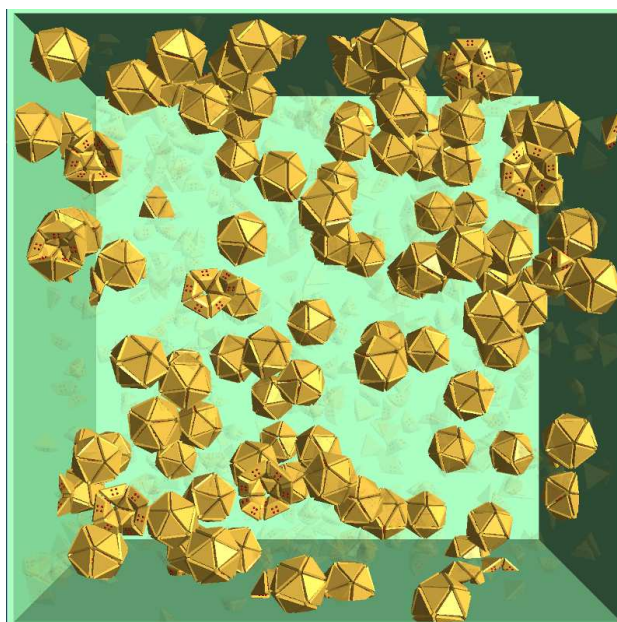


Figure 12. (Color online) Image of a system (see text) with 105 complete shells; the remaining particles are shown semi-transparently and the solvent is omitted (apparently open shells are visual artifacts due to periodic boundaries).

3.4. Growth events

The growth histories of individual shells can be followed, but this requires associating partial assemblies at different stages of the run with particular shells at run's end. Since particles join and leave different growing clusters, sometimes multiple times, the relevant cluster is the one having maximum population overlap with the final shell. The criterion is not perfect, since a given final shell can own the majority of particles from more than one smaller early cluster, and the identity of the cluster containing the most particles destined for a given shell can change; but events of this kind generally have only minimal influence on the ability to monitor individual cluster histories once a relatively stable core has formed, and they become even less of a concern at more advanced stages of growth. Cluster analysis considers all the current members, including particles that subsequently detach.

The growth histories of a subset of 20 (of the total of 83) complete shells, for $e = 0.13$, are shown in Fig. 13. Initial growth to pentamer size is rapid, but subsequent growth rates exhibit a broad distribution. While there are clusters that develop rapidly – some even monotonically – to completion, the paths of others become temporarily blocked, repeatedly adding and then promptly losing an additional particle until a more lasting growth step is eventually taken.

The statistics of the different types of size-changing events offers further insight into the growth process. Fig. 14 shows the fractions of events corresponding to unit size changes in each direction, together with the fractions of all size-changing events

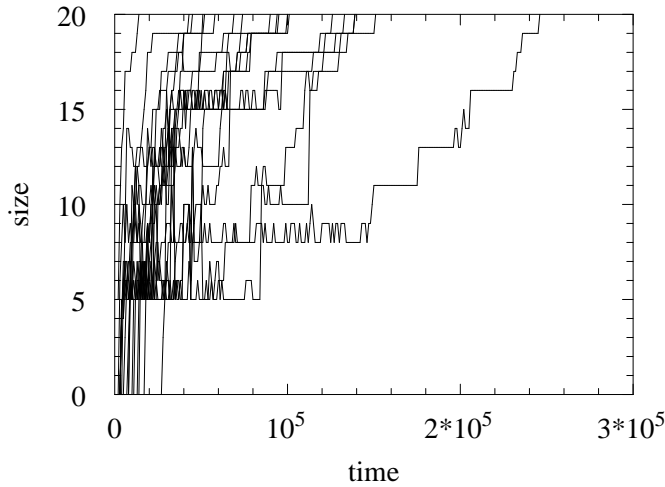


Figure 13. Size histories for 20 of the shells.

irrespective of magnitude, each as a function of cluster size. The reversible nature of the process is abundantly clear. A substantial fraction of events at nearly all sizes (excluding 5 and 19) involve size decreases. Moreover, there are cluster sizes (e.g., 7, 9, 13, 16) for which the size is actually more likely to decrease than increase. So while unit size changes tend to account for the majority of events, the process is bidirectional. This is clear evidence of the strong effect of reversibility, another key outcome of the MD simulations. The consequences of reversibility have also been considered [37] using reaction kinetics. One of the functions of reversibility is to provide a mechanism for the error correction essential to avoiding kinetic traps. The presence of reversibility is also an indication that self-assembly can occur in a near-equilibrium state, with only a slight bias in favor of growth.

Cluster lifetimes can also be measured [17]. The mean total time that clusters exist at a given size correlates with the preferred direction of size change, and is greater at those sizes where a size increase is more likely than a decrease. Owing to the reversibility of bond formation, the time a cluster spends at a particular size tends to be made up of several distinct intervals. From measurements of the mean uninterrupted time at a given size – a substantially shorter period for most sizes – it is possible to estimate the typical number of times a cluster attains that particular size; the values were found to range from a low of almost unity at size 19, up to about 15 at size five. Finally, the uninterrupted times can be examined individually according to the direction of the next size change; where there is a distinct difference, it follows the same trend as the total time. Results of this kind are further consequences of a growth process dominated by reversibility.

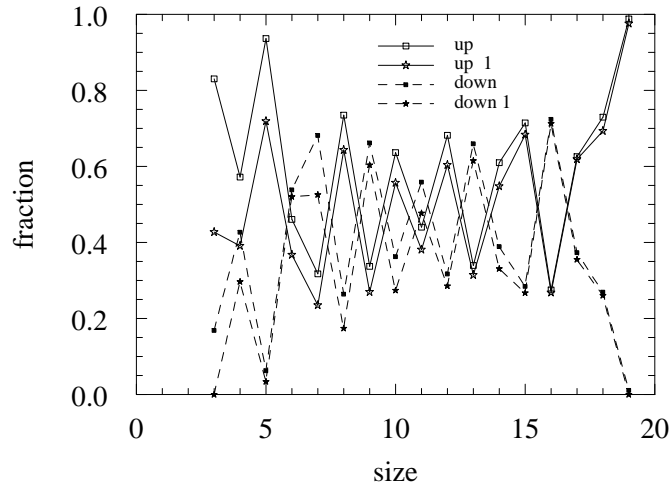


Figure 14. Fraction of size changing (up or down) events occurring for clusters of each size; unit size changes are also shown separately.

3.5. Intermediate states

The nature of the intermediate states along the growth pathways is particularly interesting [16]. Table 2 summarizes a series of measurements at 5×10^5 step intervals, for $e = 0.13$. The clusters, when grouped by bond count, reveal an extremely strong preference for maximally bonded (minimal energy) states; all the remaining clusters are within two bonds of maximum. The table includes the total numbers of possible clusters – equivalent to the distinct connected embeddings of triangles in an icosahedral lattice, quantities that are readily computed [38] – almost all of which never appear among the configurations observed. Thus, for example, while almost 92% of clusters of size 12 adopt the single 15 bond form, and the rest have either 14 or 13 bonds, none of the other 446 realizations with fewer bonds are actually observed. The effect of an imposed preference for maximally bonded intermediates has been studied with reaction kinetics [39]; the MD simulations reveal this preference to be intrinsic, another key result.

3.6. Visualizing shell assembly

Imagery is especially helpful for detailed exploration of those aspects of the growth process that are less readily quantifiable, and may suggest additional approaches for analyzing the pathway details. Fig. 15 shows a series of frames covering several stages in the growth of just one of the shells. Only the particles directly involved are included (although some may be too far away to appear in the frames). Suitable color coding, based on the known final shell membership specifies the eventual disposition of the particles: yellow for particles destined for (or already in) the final shell, gray for particles only temporarily attached to the growing shell, and green for particles that

Table 2. Intermediate states along the growth pathways (from [16]): the mean cluster fractions (f) are grouped by size (s) and bonds (b), with the maximally bonded fractions shown in bold; the numbers of distinct cluster realizations (n) are included for comparison, and the final columns enumerate the possible realizations that were not observed (sizes with unique bond counts are omitted).

s	b	n	f	Observed						Others		
				b	n	f	b	n	f	b	n	
5	5:	1	0.948	4:	5	0.052						
6	6:	1	0.953	5:	13	0.047						
7	7:	4	0.979	6:	22	0.021						
8	9:	1	0.851	8:	11	0.140	7:	46	0.009			
9	10:	3	0.938	9:	27	0.062					8:	79
10	12:	1	0.808	11:	13	0.166	10:	60	0.026		9:	151
11	13:	3	0.931	12:	28	0.069					11-10:	328
12	15:	1	0.917	14:	11	0.073	13:	74	0.010		12-11:	446
13	16:	4	0.876	15:	31	0.105	14:	142	0.019		13-12:	372
14	18:	1	0.802	17:	15	0.198					16-13:	417
15	20:	1	0.825	19:	5	0.146	18:	38	0.029		17-15:	170
16	21:	4	0.915	20:	19	0.068	19:	38	0.017		18:	28
17	23:	1	0.923	22:	7	0.077					21:	12
18	25:	1	0.888	24:	5	0.112						

are temporarily attached to yellow particles not yet in the final shell.

One such growth sequence was discussed in Ref. [17]. The sequence shown here exhibits very different behavior, with two pentamer-size clusters bonded, and after a certain period of time breaking apart, with only one destined for the final shell. Subsequently, it links up with a different pentamer and then continues to grow by smaller increments. The last frame of the sequence shows the final particle about to close the shell. Shells clearly have very distinct histories. Particles, literally, can come and go; only when bound to most of its neighbors, and embedded in a substantial portion of a partial shell, is an individual particle unlikely to be knocked out of position. Population exchanges of this kind are not readily characterized in a quantitative manner, but can be tracked visually.

3.7. Assembly of larger shells

The next stage in developing the approach is modeling the self-assembly of larger shells in a solvated environment. Current efforts are focused on pentakis-dodecahedral and T=1 shells, built from 60 triangular or trapezoidal particles, respectively. The systems contain 2750 particles, sufficient in principle for 45 shells, with other aspects of the simulations, including the interaction parameters and overall system size, remaining

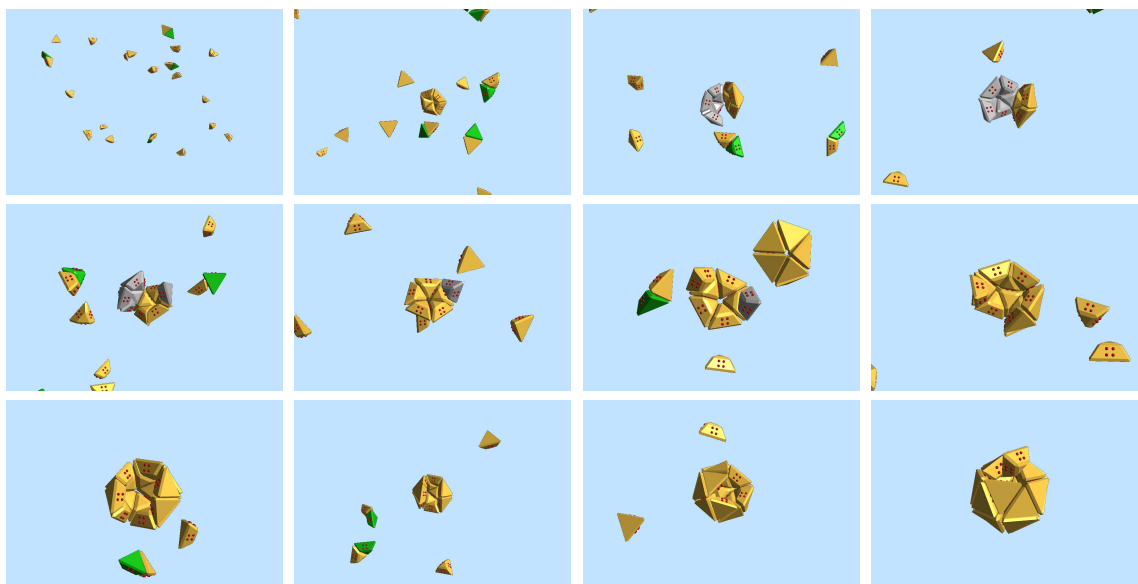


Figure 15. (Color online) Stages in the reversible growth of one of the shells, including two pentamers being temporarily bonded (upper-right frame); only the particles directly involved are included although some lie outside the field of view (solvent is not shown); the color coding is explained in the text.

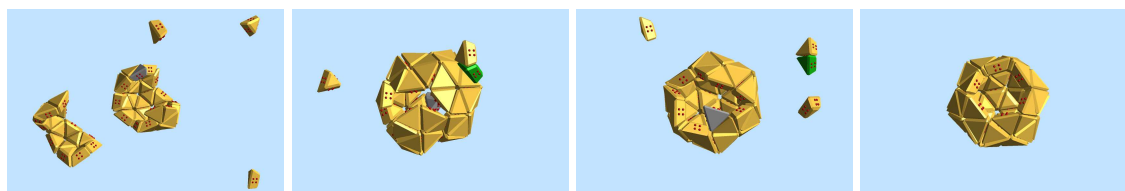


Figure 16. (Color online) Stages in the merging of two subassemblies after 20 , 21 and 22×10^6 steps, and the 54 -member, still incomplete shell after 33×10^6 steps (the color coding is the same as before).

unchanged. While growing such shells without a solvent – and therefore subject to artificial breakup and damping issues as described above – was not especially demanding computationally, the extra effort resulting from inclusion of the solvent is substantial. The simulation runs will have to be considerably longer than for the icosahedra in order to achieve respectable yields, and since the shell size is tripled, the number of particles in the system, as well as the number of solvent atoms, will eventually need to be increased accordingly, although this is not reflected in the present exploratory results.

The first of two examples of what occurs along the growth pathway is shown in Fig. 16, where two substantial subassemblies bond together. The opportunity for complex events of this kind is increased for larger shells, with reversible bonding helping to ensure – although not guaranteeing – that obstructing particles are ejected from the cluster.

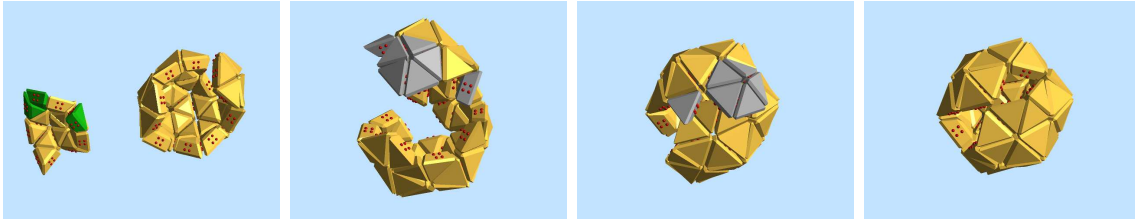


Figure 17. (Color online) Temporary formation of an incorrect structure: at 29.5×10^6 steps the main subassembly (size 41) is about to merge with a smaller piece; at 29.9×10^6 steps the merge has occurred (size 59); the cluster at 30.6×10^6 steps (size 58) with overlapping shell components clearly visible; at 34.3×10^6 steps the extra pieces have broken off leaving a cluster of size 54.

A merging event followed by serious error correction, involving a different cluster, appears in Fig. 17. As a result of the merge, the growing shell acquires an unwanted pentamer that is seen to inhibit future successful growth; it remains attached for a considerable period of time (5×10^6 steps) before breaking off and allowing the shell to continue along its growth path. The message conveyed by these two sequences reinforces the earlier evidence of cluster histories being subject to wide variation.

The final image, Fig. 18 shows the state of a system of triangular particles (at the time of writing) after 44×10^6 steps. There are 13 clusters of size ≥ 50 , including two closed shells, the first of which completed after 39×10^6 steps, and one of size 59 (none of these three correspond to the structure examined in Fig. 17). At this stage 200 monomers remain, so further shell completion appears likely. The largest shell size in an analogous simulation with trapezoidal particles was 47, after 19×10^6 steps, but the monomer supply was practically exhausted. The completion rate here is, not surprisingly, much slower than for the smaller shells which, after runs of this duration, had already yielded significant numbers of complete structures.

4. Conclusion

The present simulations provide a demonstration that a simple potential energy function, based on structural considerations, is essentially all that is required to drive self-assembly. This approach, whose focus is on examining the essential physics of the growth process, allows the influence of shape and interactions to be examined relatively easily, in contrast to the heavy computational demands required for a more detailed atomic description.

Self-assembly at submicroscopic scales, where intrinsic thermal fluctuations become important, is seen to be very different from inherently unidirectional macroscopic assembly. Reversibility makes itself felt along the entire assembly pathway, with dissociation more likely than growth throughout much of the process. The surprising aspects of the results – given the absence of any *a priori* theoretical expectations – are

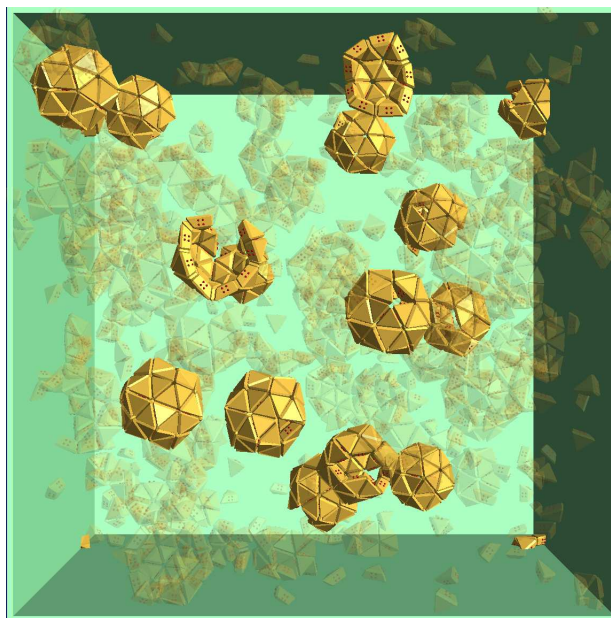


Figure 18. (Color online) Shells growing in solvent, including two that are complete (size 60); clusters with size < 50 and monomers are shown semi-transparently and the solvent is omitted.

the fast growth rates, high yields, and the avoidance of incorrect final structures.

Although the models are not representative of real capsomer proteins, and no attempt has been made to develop a more explicit relationship, if there exist universal features underlying capsid assembly, simplified systems of this kind ought to embody their essence. It goes without saying that the more general aspects of self-assembly suggested by these simulations, in particular the coexistence of reversibility with a high error-free yield, are likely to have important implications for understanding supramolecular assembly in general, and capsid formation in particular.

References

- [1] F. H. C. Crick and J. D. Watson. The structure of small viruses. *Nature (Lond.)*, 177:473, 1956.
- [2] D. L. D. Caspar and A. Klug. Physical principles in the construction of regular viruses. *Cold Spring Harbor Symp. Quant. Biol.*, 27:1, 1962.
- [3] G. M. Whitesides and B. Grzybowski. Self-assembly at all scales. *Science*, 295:2418, 2002.
- [4] D. L. D. Caspar. Movement and self-control in protein assemblies: Quasi-equivalence revisited. *Biophys. J.*, 32:103, 1980.
- [5] D. C. Rapaport. *The Art of Molecular Dynamics Simulation*. Cambridge University Press, Cambridge, 2nd edition, 2004.
- [6] D. Endres and A. Zlotnick. Model-based analysis of assembly kinetics for virus capsids and other spherical polymers. *Biophys. J.*, 83:1217, 2002.
- [7] T. S. Baker, N. H. Olson, and S. D. Fuller. Adding the third dimension to virus life cycles: Three-dimensional reconstruction of icosahedral viruses from cryo-electron micrographs. *Microbiol. Mol. Biol. Rev.*, 63:862, 1999.

- [8] J. M. Fox, J. E. Johnson, and M. J. Young. RNA/protein interactions in icosahedral virus assembly. *Sem. in Virology*, 5:51, 1994.
- [9] P. E. Prevelige, D. Thomas, and J. King. Nucleation and growth phases in the polymerization of coat and scaffolding subunits into icosahedral procapsid shells. *Biophys. J.*, 64:824, 1993.
- [10] A. Zlotnick, J. M. Johnson, P. W. Wingfield, S. J. Stahl, and D. Endres. A theoretical model successfully identifies features of hepatitis b virus capsid assembly. *Biochemistry*, 38:14644, 1999.
- [11] G. L. Casini, D. Graham, D. Heine, R. L. Garcea, and D. T. Wu. In vitro papillomavirus capsid assembly analyzed by light scattering. *Virology*, 325:320, 2004.
- [12] J. A. Speir, S. Munshi, G. Wang, T. S. Baker, and J. E. Johnson. Structure of the native and swollen forms of cowpea chlorotic mottle virus determined by x-ray crystallography and cryo-electron microscopy. *Structure*, 3:63, 1995.
- [13] J. E. Johnson. Functional implications of protein-protein interactions in icosahedral viruses. *Proc. Natl. Acad. Sci. USA*, 93:27, 1996.
- [14] D. C. Rapaport, J. E. Johnson, and J. Skolnick. Supramolecular self-assembly: Molecular dynamics modeling of polyhedral shell formation. *Comp. Phys. Comm.*, 121:231, 1999.
- [15] D. C. Rapaport. Self-assembly of polyhedral shells: A molecular dynamics study. *Phys. Rev. E*, 70:051905, 2004.
- [16] D. C. Rapaport. Role of reversibility in viral capsid growth: A paradigm for self-assembly. *Phys. Rev. Lett.*, 101:186101, 2008.
- [17] D. C. Rapaport. Studies of reversible capsid shell growth. *J. Phys.: Condens. Matter*, 22:104115, 2010.
- [18] H. D. Nguyen, V. S. Reddy, and C. L. Brooks III. Deciphering the kinetic mechanism of spontaneous self-assembly of icosahedral capsids. *Nano Letters*, 7:338, 2007.
- [19] M. F. Hagan and D. Chandler. Dynamic pathways for viral capsid assembly. *Biophys. J.*, 91:42, 2006.
- [20] R. Schwartz, P. W. Shor, P. E. Prevelige, and B. Berger. Local rules simulation of the kinetics of virus capsid self-assembly. *Biophys. J.*, 75:2626, 1998.
- [21] A. W. Wilber, J. P. K. Doye, A. A. Louis, E. G. Noya, M. A. Miller, and P. Wong. Reversible self-assembly of patchy particles into monodisperse icosahedral clusters. *J. Chem. Phys.*, 127:085106, 2007.
- [22] T. Chen, Z. Zhang, and S. C. Glotzer. A precise packing sequence for self-assembled convex structures. *Proc. Natl. Acad. Sci. USA*, 104:717, 2007.
- [23] I. G. Johnston, A. A. Louis, and J. P. K. Doye. Modelling the self-assembly of virus capsids. *J. Phys.: Condens. Matter*, 22:104101, 2010.
- [24] P. L. Freddolino, A. S. Arhipov, S. B. Larson, A. McPherson, and K. Schulten. Molecular dynamics simulations of the complete satellite tobacco mosaic virus. *Structure*, 14:437, 2006.
- [25] J. Lidmar, L. Mirny, and D. R. Nelson. Virus shapes and buckling transitions in spherical shells. *Phys. Rev. E*, 68:051910, 2003.
- [26] R. Twarock. A tiling approach to virus capsid assembly explaining a structural puzzle in virology. *J. Theor. Biol.*, 226:477, 2004.
- [27] R. Zandi, D. Reguera, R. F. Bruinsma, W. M. Gelbart, and J. Rudnick. Origin of icosahedral symmetry in viruses. *Proc. Natl. Acad. Sci. USA*, 101:15556, 2004.
- [28] S. D. Hicks and C. L. Henley. Irreversible growth model for virus capsid assembly. *Phys. Rev. E*, 74:031912, 2006.
- [29] M. Hemberg, S. N. Yaliraki, and M. Barahona. Stochastic kinetics of viral capsid assembly based on detailed protein structures. *Biophys. J.*, 90:3029, 2006.
- [30] P. van der Schoot and R. Zandi. Kinetic theory of virus capsid assembly. *Phys. Biol.*, 4:296, 2007.
- [31] R. Williams. *The Geometric Foundation of Natural Structure*. Dover Publications Inc., NY, 1979.
- [32] S. Casjens. An introduction to virus structure and assembly. In S. Casjens, editor, *Virus Structure and Assembly*, page 1. Jones and Bartlett, Boston, 1985.

- [33] M. G. Rossmann and J. W. Erickson. Structure and assembly of icosahedral shells. In S. Casjens, editor, *Virus Structure and Assembly*, page 30. Jones and Bartlett, Boston, 1985.
- [34] V. S. Reddy, H. A. Giesing, R. T. Morton, A. Kumar, C. B. Post, C. L. Brooks III, and J. E. Johnson. Energetics of quasiequivalence: Computational analysis of protein-protein interactions in icosahedral viruses. *Biophys. J.*, 74:546, 1998.
- [35] A. Zlotnick, R. Aldrich, J. M. Johnson, P. Ceres, and M. J. Young. Mechanism of capsid assembly for an icosahedral plant virus. *Virology*, 277:450, 2000.
- [36] S. Singh and A. Zlotnick. Observed hysteresis of virus capsid disassembly is implicit in kinetic models of assembly. *J. Biol. Chem.*, 278(20):18249, 2003.
- [37] A. Zlotnick. To build a virus capsid, an equilibrium model of the self assembly of polyhedral protein complexes. *J. Mol. Biol.*, 241:59, 1994.
- [38] D. C. Rapaport. Algorithms for lattice statistics. *Computer Phys. Repts.*, 5:265, 1987.
- [39] D. Endres, M. Miyahara, P. Moisant, and A. Zlotnick. A reaction landscape identifies the intermediates critical for self-assembly of virus capsids and other polyhedral structures. *Protein Sci.*, 14:1518, 2005.